Optics Letters

Formation of uniform two-dimensional subwavelength structures by delayed triple femtosecond laser pulse irradiation

Sohail A. Jalil,[1,2,4] Jianjun Yang,[1,6] Mohamed Elkabbash,[4] Yuhao Lei,[1] Wanlin He,[1,3] and Chunlei Guo[1,4,5]

[1]GPL, State Key Laboratory of Applied Optics, Changchun Institute of Optics, Fine Mechanics and Physics, Chinese Academy of Sciences, Changchun 130033, China
[2]University of Chinese Academy of Sciences, Beijing, 100049, China
[3]School of Science, Xi'an Shiyou University, Xi'an, Shaanxi 710065, China
[4]The Institute of Optics, University of Rochester, Rochester, New York 14627, USA
[5]e-mail: guo@optics.rochester.edu
[6]e-mail: jjyang@ciomp.ac.cn

Received 18 February 2019; revised 3 April 2019; accepted 4 April 2019; posted 5 April 2019 (Doc. ID 360396); published 25 April 2019

The fabrication of subwavelength two-dimensional (2D) structures on metals is of paramount importance to modern nanophotonics. Here we report a method to fabricate 2D conic structures on nickel surfaces using a single beam with three temporally delayed pulses. The 2D structures are fabricated over the entire irradiated region with relatively high uniformity. By controlling the delay between the three pulses, we control the effect of each pulse in creating laser-induced periodic surface structures which enables the control of the 2D structure features, namely, the period and structure dimensions. We explain the results based on the surface plasmon polariton-femtosecond laser interference model.

https://doi.org/10.1364/OL.44.002278

Creating subwavelength structures is the cornerstone of modern photonics where structures can manipulate the effective optical properties of materials. However, a major hurdle facing nanophotonics is the high fabrication costs and low throughput of top-down fabrication methods [1], and the lack of reproducibility and uniformity of bottom-up fabrication methods [2]. On the other hand, femtosecond lasers can alter the optical, electrical, and mechanical properties of materials [3]. Particularly, the formation of laser-induced periodic surface structures (LIPSSs) promises large-area, single-step, maskless fabrication of surface structures [4]. This technique has been performed on a variety of materials, including metals [5], semiconductors [6], and dielectrics [7]. The strong dependence of LIPSSs on experimental conditions, e.g., laser parameters, material properties, and ambient environment, reflects the complexity of the physical phenomena involved and the rich possibilities of this fabrication method [3,8,9].

The majority of literature on LIPSSs, however, focuses on the formation of periodic one-dimensional (1D) structures, and recent works demonstrated uniform, large-area 1D LIPSSs [10,11]. Two-dimensional (2D) LIPSSs have the potential to be adopted for large-scale fabrication for plasmonic nano-antennas [12], photonic crystals, anti-reflection structures [13], and biomimetic surfaces [8]. The reported 2D LIPSSs, however, lacked uniformity and overall periodicity [14]. Furthermore, 2D triangular structures were created using single-pulsed, circularly polarized light [15].

Using double, temporally delayed femtosecond laser pulses was shown to enhance the efficacy of laser ablation compared to single pulses, even if the net fluence of the double pulses is equal to that of the single pulse [16]. It was later shown that using linearly polarized double pulses can create 2D structures when the polarization angle between the pulses is $>60°$, and the delay time between the pulses is sufficiently large >2 ps [17]. These 2D structures were significantly more uniform [17]. However, the 2D structures were formed only within a small portion of the irradiated region.

We note here that multi-pulsed femtosecond laser fabrication differs from traditional laser interference lithography which can create 2D structures due to multi-beam interference [18]. Multi-pulsed LIPSSs, however, are not due to the interference of the incident pulses, but rather the spatial distribution of the deposited energy by individual pulses.

Here we study the effect of triple, temporally delayed, femtosecond laser pulses on the formation of 2D LIPSSs on a nickel (Ni) surface. In contrast to using only two laser pulses, using three pulses creates uniform 2D LIPSSs over the entire irradiated area ($\sim$50 μm in our case). The three pulses are mutually orthogonal and are temporally delayed using two separate delay lines. By varying the delay time between the pulses, we find optimal conditions for creating large-area, uniform 2D conic structures with subwavelength periodicities and features. We explain the results based on the surface plasmon polariton-femtosecond laser interference model.

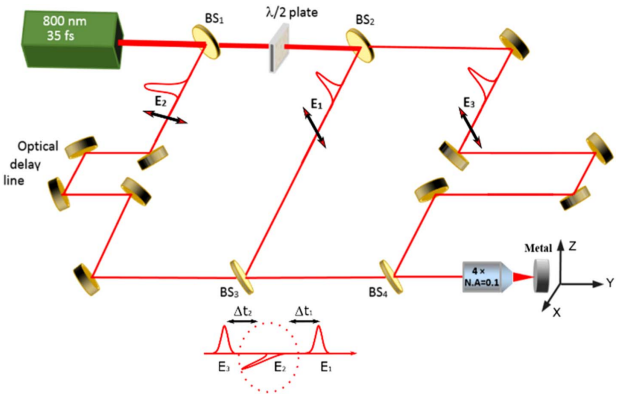

Fig. 1. Schematic of the triple-pulsed femtosecond laser processing setup. We use three temporally delayed collinear femtosecond laser beams (E_1, E_2, and E_3) with linear polarizations using two optical delay lines. E_2 polarization is orthogonal to E_1 and E_3 polarizations. Δt_1 and Δt_2 are the time delays of three laser beams arriving onto the target. The double arrows denote the polarization directions of the laser beams.

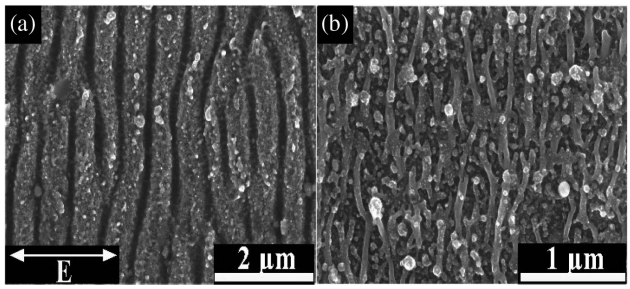

Fig. 2. SEM images of LIPSSs on the Ni surface using (a) a single-pulsed femtosecond laser beam with fluence $F = 0.21$ J/cm^2. (b) Irradiation of a collinear triple-pulsed femtosecond laser at the time delays of $\Delta t_1 = \Delta t_2 = 0$ ps with each identical energy fluence of $F = 0.07$ J/cm^2, where two laser beams were linearly polarized in the vertical direction and one beam in the horizontal direction.

A diagram of the experimental setup is illustrated in Fig. 1, where a Ti:sapphire femtosecond laser amplifier (Spectra Physics HP-Spitfire) was employed as an irradiation source to deliver horizontally polarized pulse trains at the repetition rate of 1 kHz, with a central wavelength, $\lambda = 800$ nm, and a time duration, $\tau = 35$ fs. The maximum pulse energy delivered by the laser system is 7 mJ. First, the output laser beam was divided into three parts (E_1, E_2, and E_3) with the equal energy by two splitters, BS_1 and BS_2. A half-wave plate ($\lambda/2$) inserted before the splitter BS_2 was employed to change the laser polarizations of both E_1 and E_3 into the vertical direction, whereas the laser polarization of E_2 was always kept along the horizontal direction. In addition, two optical delay lines were applied to introduce two delay times, between the first and second pulses Δt_1, and the second and third pulses Δt_2, within the beam paths of E_2 and E_3, to allow the control over the temporal delay between the three pulses. After the beam splitters BS_3 and BS_4, the three laser beams were aligned to collinear propagation and then focused by an objective lens (4×, $N.A = 0.1$) at normal incidence. A bulk Ni plate (with 10 mm in diameter and 2 mm in thickness) was mounted on a three-dimensional (3D) precision translation stage. Ni was chosen due to its attractive properties, e.g., high Curie temperature and superior magneto-restrictive properties with many potential applications such as a cathode for water purification and field emission enhancement [19,20]. To avoid excessive damage by strong laser ablation, the mechanically polished sample surface was placed 300 μm away from the laser focus along the direction reverse to the beam propagation. The sample was translated at a fixed speed of 0.35 mm/s for all experiments, resulting in approximately 172 triple laser pulses partially overlapped within one spot area. Under our experimental conditions, the lowest laser energy fluence (F) necessary to create LIPSSs on the entire irradiated spot with a single-pulsed beam is $F = 0.21$ J/cm^2. Accordingly, throughout our experiments, when using triple-pulsed beams, the fluence of the individual beam is $F = 0.07$ J/cm^2. After the laser microstructuring process, the surface morphological features were analyzed by both scanning electron microscopy (SEM) and atomic force microscopy (AFM).

First, for the purpose of comparison, the surface morphology induced by a single-pulsed femtosecond laser beam is demonstrated in Fig. 2(a) with $F = 0.21$ J/cm^2. The obtained result clearly shows the formation of LIPSSs with a groove periodicity of about (630 ± 50) nm . The spatial orientation of low-spatial frequency LIPSSs (LSFL) is perpendicular to the incident laser polarization [marked by the double-headed arrow "E" in Fig. 2(a)], which is a common observation in previous studies [5]. The formation of 1D LIPSSs is conventionally understood as a result of the interaction between the incident light and the surface scattering wave from surface roughness, namely, surface plasmon polaritons (SPPs) [21,22]. The single-beam LIPSSs show low uniformity due to random structure initiation from random scatterers [11].

On the other hand, the double-pulsed femtosecond laser beam is more efficient for material ablation, as long the delay time between the two pulses is ~ 1 ps $< \Delta t < 10$ ps. For delay times below 1 ps, the absorbed energy is yet to be transferred to the lattice via electron-phonon coupling. For delay times greater than 10 ps, the ablation efficiency drops due to heat and carrier diffusion, reducing the volumetric energy density deposited by the first pulse into the material and due to plasma shielding effects, where the material ablated by the first pulse partially absorbs the radiation of the second pulse [23]. When using a train of triple-pulsed femtosecond lasers with no time delay between the first, second, and third pulses ($F_1 = F_2 = F_3 = 0.07$ J/cm^2), i.e., $\Delta t_1 = \Delta t_2 = 0$ and orthogonal polarizations between "(E_1, E_3) and E_2", we observe a random distribution of nanowires and nanoparticles with no uniform periodic structures, likely due to excessive melting from the constructive interference (0.28 J/cm^2) between the first and third pulses [Fig. 2(b)], and the net fluence becomes 0.35 J/cm^2.

However, by introducing a delay between the three pulses, large-area, 2D periodic structures are formed. Figure 3(a) shows the surface morphology obtained at time delays $\Delta t_1 = 42$ ps and $\Delta t_2 = 50$ ps, i.e., E_2 and E_3 are delayed by 42 and 92 ps, respectively, with respect to E_1. Uniform 2D structures are formed over the entire irradiated region ~50 μm, including the center and peripheries [Fig. 3(a)]. The regular alignment along the scanning direction indicates an indefinite extension

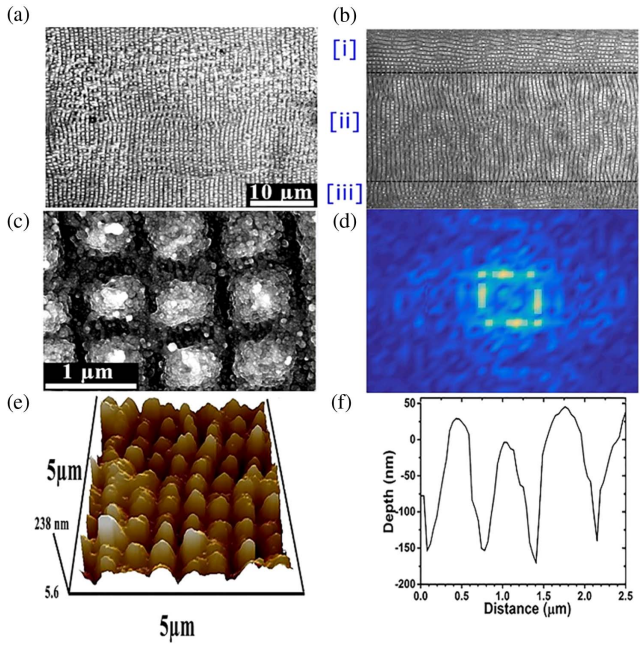

Fig. 3. (a) SEM image of 2D uniform conic structures by irradiation of three temporally delayed collinear femtosecond laser pulses and its formation on overall laser scanned areas, where the experimental conditions are $\Delta t_1 = 42$ ps, $\Delta t_2 = 50$ ps, and the total laser energy fluence is $F = 0.21$ J/cm^2. (b) Comparison of surface structures formed, using two temporally delayed pulses at $\Delta t = 10$ ps and $F = 0.21$ J/cm^2, where 1D and 2D structures formed with different orientations in the center and peripheries of the scanned line; the scale-bar of 10 μm is the same for (a) and (b); (c) zoom-in view of 3(a). (d) Image of fast Fourier transform of the 2D structure arrays in (c). (e) 3D topographic view of the fabricated structures measured with AFM. (f) Cross-sectional line profile of the modulation depth for the structure.

of these structures via sample translation. Note that uniform 2D periodic arrays were produced previously using a double-pulsed femtosecond laser with orthogonal polarizations; however, the structures formed only within the center of the scanned region of a double-pulsed beam (~6 μm) [17]. A comparison of 2D conic structures formed using temporally delayed double pulses at $\Delta t = 10$ ps and $F = 0.21$ J/cm^2 is also shown in Fig. 3(b), where 1D and 2D structures with different orientations in the center and peripheries of the scanned line can be seen. The black dotted lines corresponding to the region (i-iii) show different orientations, as well as 1D and 2D structures. Figure 3(c) shows a zoom-in view of Fig. 3(a), and corresponding 2D fast Fourier transform is shown in Fig. 3(d), where the distinct bright spots reflect the spatial distribution features of the 2D conic structures in different directions. The obtained topographical AFM image in Fig. 3(e) demonstrates a 3D view of the formed structures. The conic structures have an average width of ~520 nm, i.e., the structures are subwavelength. The average modulation, peak-to-valley, depth is estimated from the surface cross-sectional profiles [Fig. 3(f)] and is ~170 nm.

To gain a deeper understanding of the triple-pulsed beam ablation process, we investigated the effect of changing the delay time on the surface structure formation. We changed

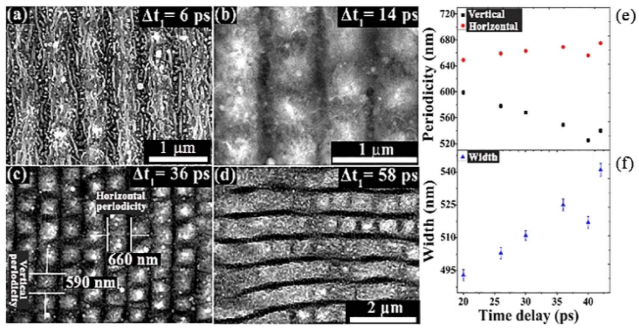

Fig. 4. (a)–(d) Evolution of subwavelength conic structures with varying the time delays Δt_1 within a range of 0–58 ps at a constant Δt_2 of 50 ps. The scale bar is 2 μm for (c) and (d). (e) and (f) Measured feature sizes of the 2D surface structures as a function of the time delay $\Delta t_1 = 20$–42 ps for the uniform region. (e) Spatial periodicities in both the horizontal and vertical directions. (f) Width of individual conic structures.

Δt_1 from 0–58 ps while keeping Δt_2 at 50 ps, $F_1 = F_2 = F_3 = 0.07$ J/cm^2, and the scanning speed at 0.35 mm/s. At short delay times, i.e., 1 ps $< \Delta t_1 <$ 20 ps, clear 1D LIPSSs, along with nanowires, are formed orthogonal to E_2 polarization [Figs. 4(a) and 4(b)]. At intermediate delay times, i.e., 20 ps $< \Delta t_1 <$ 42 ps, 2D conic structures are formed, and the grooves become more defined as a function of Δt_1 [Fig. 4(c)]. Finally, at long delay times, i.e., 46 ps $< \Delta t_1 <$ 58 ps, 1D LIPSSs are formed orthogonal to E_1 and E_3 [Fig. 4(d)]. Accordingly, the optimal delay to create the 2D conic structures is the intermediate delay times.

The results can be understood in the framework of LIPSS formation due to SPP laser interference [3,9], and by the superior performance of multiple-pulsed trains for efficient ablation [23]. In general, 1D LIPSSs are formed with grating lines orthogonal to the incident light polarization [3]. For the triple-pulsed beam systems and short delay times, the ablation efficiency of the second beam effect is prevalent, because Δt_1 is very short, while Δt_2 is relatively long leading to clear grooves orthogonal to E_2 [Fig. 4(a)]. On the other hand, for long delay times, we only observe grooves orthogonal to E_1 and E_3 [Fig. 4(d)]. Since the fluence of individual pulses is insufficient to create LIPSSs, the energy acquired by the lattice from previous pulses is necessary for the subsequent pulse to create grooves. In the case of long delay times, the energy imparted by E_1 has been partially diffused, via phonon–phonon scattering, which means that E_2 is not capable of creating grooves. However, E_3 can create LIPSSs due to the additional energy imparted by E_2.

Figure 4(e) shows change in the 2D periodicity along the vertical and horizontal directions as a function of Δt_1 for 20 ps $< \Delta t_1 <$ 42 ps, where we obtained the most uniform structures. For Figs. 4(e) and 4(f), the error bars are calculated as the standard deviation of multiple periods and structures by inspecting the SEM images. We note here that the horizontal periodicity corresponds to the vertical grooves which are formed orthogonal to E_2 polarization, while the vertical periodicity [Fig. 4(c)] corresponds to the horizontal grooves which are formed orthogonal to E_1 and E_3 polarization. While the horizontal periodicity remains relatively constant, the vertical periodicity decreases for longer Δt_1. To understand the period

dependence on Δt_1, we recall that the formation of LSFL is generally understood to be due to the interference between SPPs and the incident laser beam, and is given by, $\boldsymbol{G} = \boldsymbol{k_i} - \boldsymbol{k_{SPP}}$ [9,24], where $\boldsymbol{G}$ is the groove wave-vector produced due to the interference; $\boldsymbol{k_i} = 2\pi|\lambda_i|^{-1}$ and $\boldsymbol{k_{SPP}} = 2\pi|\lambda_{SPP}|^{-1}$ are the incident laser beam and the SPP wave-vectors, respectively; and λ_i and λ_{SPP} are the incident laser wavelength and SPP wavelength, respectively. The groove period is given by $\Lambda = 2\pi|\boldsymbol{G}|^{-1} = \lambda_i/(\frac{\lambda_i}{\lambda_{SPP}} \pm \sin\theta)$, where θ is the angle of incident light measured from the normal [3,8,9,24]. For normal incidence, as in our case, this yields $\Lambda = \lambda_{SPP}$. For metals, the complex permittivity is given by $\tilde{\varepsilon} = \varepsilon_m^{Re} + i\varepsilon_m^{Im}$, where, ε_m^{Re} and ε_m^{Im} are the real and imaginary parts of the metallic permittivity, respectively. The confinement of SPP waves at the metal-dielectric interface requires a phase mismatch with free space radiation which makes the SPP wavelength highly sensitive to ε_m^{Re} and the dielectric permittivity (ε_D) such that $\lambda_{SPP} = \lambda_i\left(\frac{\varepsilon_m^{Re}+\varepsilon_D}{\varepsilon_m^{Re}\varepsilon_D}\right)^{1/2}$. Given that vertical periodicity is orthogonal to the polarization of E_1 and E_3, the delay between the two pulses should determine the SPP wave-vector and, consequently, the groove period.

For long delay times, ε_m^{Re} decreases; consequently we believe that this leads to a decrease in λ_{SPP} which creates a shorter groove period [9]. The decrease in ε_m^{Re} for longer delay times is due to the decrease in the excited electron density that is locally excited by E_1. On the other hand, the horizontal periodicity is insensitive to the introduced delay, as it is caused by the second pulse [16]. We also note that the width of the conic structures increases for longer delays, as shown in Fig. 4(f). The temperature-dependent surface tension and recoil pressure are capable of generating molten materials movement that may lead to an observed increase in width of conic structures as a function of delay time [25,26]. Accordingly, the delay time between the three pulses enables some control over the formed structure parameters.

To conclude, we demonstrated that 2D periodic surface structures can be produced on large areas using three temporally delayed pulsed beams. The method allows for controlling the periodicity of subwavelength structures by only changing the time delay and differs from conventional laser interference lithography.

Using a triple-pulsed beam allows for additional degrees of freedom that can enable the control over different structural parameters. The proposed method can be used on harder metals, e.g., tungsten carbide, to create molds that can be used on polymers to create anti-reflection moth eye structures. In addition, creating the same structures on plasmonic metals, e.g., silver or gold, may enable the direct fabrication of type-I hyperbolic metamaterials [27], as well as transition hyperbolic metamaterials [28].

Funding. Bill and Melinda Gates Foundation (OPP1119542).

REFERENCES

1. M. ElKabbash, E. Ilker, T. Letsou, N. Hoffman, A. Yaney, M. Hinczewski, and G. Strangi, Opt. Lett. **42**, 3598 (2017).
2. G. M. Whitesides and B. Grzybowski, Science **295**, 2418 (2002).
3. A. Y. Vorobyev and C. Guo, Laser Photonics Rev. **7**, 385 (2013).
4. L. Wang, Q.-D. Chen, X.-W. Cao, R. Buividas, X. Wang, S. Juodkazis, and H.-B. Sun, Light: Sci. Appl. **6**, e17112 (2017).
5. A. Vorobyev, V. Makin, and C. Guo, J. Appl. Phys. **101**, 034903 (2007).
6. G. Miyaji, K. Miyazaki, K. Zhang, T. Yoshifuji, and J. Fujita, Opt. Express **20**, 14848 (2012).
7. Y. Shimotsuma, P. G. Kazansky, J. Qiu, and K. Hirao, Phys. Rev. Lett. **91**, 247405 (2003).
8. J. Bonse, S. Höhm, S. V. Kirner, A. Rosenfeld, and J. Krüger, IEEE J. Sel. Top. Quantum Electron. **23**, 109 (2017).
9. M. Huang, F. Zhao, Y. Cheng, N. Xu, and Z. Xu, ACS Nano **3**, 4062 (2009).
10. S. A. Jalil, J. Yang, M. ElKabbash, S. C. Singh, and C. Guo, Appl. Surf. Sci. **471**, 516 (2019).
11. B. Öktem, I. Pavlov, S. Ilday, H. Kalaycıoğlu, A. Rybak, S. Yavaş, M. Erdoğan, and F. Ö. Ilday, Nat. Photonics **7**, 897 (2013).
12. A. M. Schwartzberg, T. Y. Olson, C. E. Talley, and J. Z. Zhang, J. Phys. Chem. B **110**, 19935 (2006).
13. S. Wilson and M. Hutley, Opt. Acta **29**, 993 (1982).
14. K. Ahmmed, C. Grambow, and A.-M. Kietzig, Micromachines **5**, 1219 (2014).
15. J.-M. Romano, A. Garcia-Giron, P. Penchev, and S. Dimov, Appl. Surf. Sci. **440**, 162 (2018).
16. S. Höhm, M. Herzlieb, A. Rosenfeld, J. Krüger, and J. Bonse, Appl. Surf. Sci. **374**, 331 (2016).
17. J. Cong, J. Yang, B. Zhao, and X. Xu, Opt. Express **23**, 5357 (2015).
18. Z. Zhang, Z. Wang, D. Wang, and Y. Ding, J. Laser Appl. **26**, 012010 (2014).
19. S. Jalil, S. Bashir, M. Akram, Q. Ahmed, and F. Haq, Indian J. Phys. **91**, 953 (2017).
20. Y. Zhu, T. Liu, L. Li, S. Song, and R. Ding, Ionics **24**, 1121 (2018).
21. H. Van Driel, J. Sipe, and J. F. Young, Phys. Rev. Lett. **49**, 1955 (1982).
22. J. F. Young, J. Preston, H. Van Driel, and J. Sipe, Phys. Rev. B **27**, 1155 (1983).
23. A. Rosenfeld, S. Höhm, J. Krüger, and J. Bonse, *Encyclopedia of Interfacial Chemistry: Surface Science and Electrochemistry* (Elsevier, 2017), pp. 338–347.
24. F. Keilmann and Y. Bai, Appl. Phys. A **29**, 9 (1982).
25. G. D. Tsibidis, M. Barberoglou, P. A. Loukakos, E. Stratakis, and C. Fotakis, Phys. Rev. B **86**, 115316 (2012).
26. G. D. Tsibidis, C. Fotakis, and E. Stratakis, Phys. Rev. B **92**, 041405 (2015).
27. K. V. Sreekanth, M. ElKabbash, Y. Alapan, E. I. Ilker, M. Hinczewski, U. A. Gurkan, and G. Strangi, EPJ Appl. Metamater. **4**, 1 (2017).
28. B. Wells, Z. A. Kudyshev, N. Litchinitser, and V. A. Podolskiy, ACS Photonics **4**, 2470 (2017).